Available online at www.sciencedirect.com
SCIENCE DIRECT®
PERGAMON
International Journal of Heat and Mass Transfer 46 (2003) 1265–1278
International Journal of HEAT and MASS TRANSFER
www.elsevier.com/locate/ijhmt

# Aerodynamic and mass transfer characteristics of an annular bistable impinging jet with a fluidic flip–flop control

Zdeněk Trávníček [a,*], Kazimierz Peszyński [b], Jan Hošek [a], Sylwester Wawrzyniak [b]

[a] *Institute of Thermomechanics, Czech Academy of Sciences, Dolejškova 5, 182 00 Prague 8, Czech Republic*
[b] *Department of Control and Machinery Design, Faculty of Mechanical Engineering, University of Technology and Agriculture, Kaliskiego 7, 85–791 Bydgoszcz, Poland*

Received 10 June 2002

**Abstract**

An annular nozzle has been designed on the basis of fluidic principles. The nozzle forms actively controlled air jet. Numerical and experimental investigations were performed in several subsequent steps, namely numerical simulation (using a commercial CFD code FLUENT), geometry adaptation, models manufacturing, flow visualization, hot-wire measurement, and mass transfer (naphthalene sublimation) experiment. A "jet switching" possibility has been discussed, an undesirable hysteresis effect has been suppressed. Present collaborative numerical and experimental investigations have resulted in a better understanding of mechanisms involved in controlled impinging jets, as well as in a further improvement of the particular nozzle geometry.


## 1. Introduction

### 1.1. Impinging jets

Heat and mass transfer between surface areas and their surroundings are frequently carried out by fluid jets impinging on surfaces. The topic has been a subject of numerous studies over the past four decades, the most important results were summarized, e.g., in an outstanding monograph by Dyban and Mazur [1], and in an exceptional work by Martin [2]. Several comprehensive reviews have appeared periodically up to the present time, such as [3–8]. Theoretical, experimental and numerical research of the topic continues perpetually—see, e.g., a recent review by Garimella [8], and one of the recent experimental studies [9].

Great stimulation of this effort comes from industrial applications, oriented to a heat transfer enhancement by means of impinging jets. The most important applications of impinging submerged jets, when a working fluid is gas, are summarized in Table 1. Three typical advantages of impinging jet applications are (1) high intensity of heat/mass transfer, (2) good adaptability to a different surface shape with good localization of heat/mass transfer surface area, and (3) relatively simple and cost-effective applications.

This paper is focused on the *impinging air jet,* free-surface (liquid) jets are evidently different case. Note that a classification *submerged jet–free-surface jet* has been used, e.g., by Webb and Ma [7] and Garimella [8], and seems to be rather logical. However, a terminology according to a recent heat transfer leading review [10], which is significant, sounds surprisingly as *submerged jet–liquid jet*. Former term is used in [10] for "air issuing into air, liquid issuing into liquid", later term for "a jet in which the issuing stream has density significantly higher than that of the ambient fluid". On the other hand, many authors use quite common expressions *submerged jet–free jet*, such as Herman [11].

Fluid mechanics of impinging jets and resultant heat transfer onto exposed surfaces were investigated in

* Corresponding author. Tel.: +420-2-6605-3302; fax: + 420-2-8658-4695.
*E-mail address:* tr@it.cas.cz (Z. Trávníček).

0017-9310/03/$ - see front matter © 2002 Elsevier Science Ltd. All rights reserved.
PII: S0017-9310(02)00381-2

**Nomenclature**

| | |
|---|---|
| $d$ | inner diameter of annular nozzle, $d = 74$ mm (see Fig. 1) |
| $D$ | outer diameter of annular nozzle, $D = 84$ mm (see Fig. 1) |
| $D_n$ | mass diffusion coefficient of naphthalene vapor in air |
| $h$ | local heat transfer coefficient |
| $h_m$ | local mass transfer coefficient |
| $H$ | nozzle-to-wall spacing (see Fig. 8) |
| $k$ | turbulent kinetic energy |
| $Q$ | volumetric flow rate |
| $r$ | radial coordinate (see Fig. 1) |
| $r_c$ | dimensionless control flow rate, $Q_c/Q_j$ |
| $Re_D$ | Reynolds number of annular jet outer diameter at nozzle exit, $U_j D/v$ |
| $Re_W$ | Reynolds number of annular slot jet width at nozzle exit, $U_j W/v$ |
| $Sc$ | Schmidt number for naphthalene in air, $v/D_n$ |
| $Sh_D$ | Sherwood number, $h_m D/D_n$ |
| $T$ | temperature |
| $U$ | mean velocity |
| $W$ | slot width of the main (annular) nozzle, $(D-d)/2$ |
| $x$ | axial coordinate (see Fig. 1) |

*Greek symbols*

| | |
|---|---|
| $\Delta_c$ | slot width of the control nozzle, $\Delta_c = 0.5$ mm (see Fig. 1) |
| $\Delta\tau$ | run time duration of the naphthalene sublimation |
| $\Delta x$ | sublimation depth of naphthalene |
| $\varepsilon$ | turbulent kinetic energy dissipation rate |
| $v$ | kinematic viscosity of air |
| $\rho$ | density of air |

*Subscripts*

| | |
|---|---|
| c | control jet from a radial slot of a width $\Delta_c$ (see Fig. 1) |
| j | main jet from the annular nozzle of diameters $D$, $d$ (see Fig. 1) |
| n | naphthalene |
| s | spoiler |
| w | surface of the exposed wall |

Table 1
Main applications of impinging submerged jets

Cooling
- Thermal control of high-heat-dissipation electronic components
- Turbine blades
- Combustion chambers
- Furnace refractory walls
- High heat flux surfaces in fusion reactors
- Sheet glass cooling, annealing and tempering
- Thermal treatment of materials in rolling mills, cooling and annealing of metal and plastic sheets

Heating
- Flame impingement heating, combustion phenomena
- Aircraft thermal de-icing systems
- Precise control of a cylinder temperature in paper-making industry

Drying technology of various material
- Paper (paper-making industry, cardboard, sticking tape; print lines)
- Textile (fabrics in thermo-fixing stenters, etc.)
- Veneer and plywood
- Films
- Ceramics and porcelain; plates
- Coated sheet metal
- Thin sheet metal, as well as thick rolled products

Manufacturing of thin film transistor-liquid crystal display panels

Test case for the CFD, typically for turbulence models validation

many variants of nozzle geometry, basic configurations use round and slot nozzles and their various modifications. A design of new nozzle systems aimed at heat transfer enhancement is typically jointed with specifically shaped nozzles such as annular, elliptic, square, oblong, triangle, and rosette shaped ones. Another ex-

ample of more complex "specialty nozzles" is the radial jet reattachment nozzle [12]—an annular nozzle with a predominantly radial orientation of an exit slot, which spreads the jet impingement over a large surface area.

### 1.2. Impinging multi-stable jets, and the present work motivation

Flow fields of impinging jets are commonly classified as complex flows even at a basic nozzle geometry because they consist of many tasks bound together (flow development in a nozzle, jet flow, jet shear layer, stagnation flow, wall jet in laminar, transitional and fully turbulent regimes, etc.). The present paper was undertaken to provide an insight into an impinging jet problem, which still seems relatively far from the main research field, namely impinging multi-stable jets. Basic idea lies in a combination of *impinging jets* with a *jet control* by means of *fluidic principles*.

An annular impinging jet was studied numerically by Kokoshima et al. [13], and a bistable behavior (called in [13] as "closed and opened flow patterns") was predicted including a hysteresis character. Experimental investigation of annular impinging jets was presented by Maki and Yabe [14]; four flow regimes were identified, and three of them were characterized as a recirculating unsteady flow. The phenomenon was confirmed experimentally by Trávníček and Křížek [15] for a planar geometry; the paper [15] is probably the first publication on the bistability and hysteresis of impinging jets in a reviewed journal at all. A two-dimensional impinging jet from a two-slot-nozzle (slot nozzle which is halved by a partition bar) has been investigated, and bistable switching and hysteresis effects were studied experimentally (flow visualization, measurements of pressure, and mass transfer). An advanced variant of the nozzle geometry has been studied by Trávníček and Maršík [16].

Recent study by Tesař [17] presents an annular jet, when five flow regimes were identified by a numeric simulation, including bistability on a demarcation between two of them. Surprisingly, no hysteresis was referred to in [17]—the phenomenon is, apparently, not common but it depends on a specific geometry.

The term *fluidics* means a technology of flow handling based on the fluid flow interaction without action of moving components. It was investigated during the past 40 years mainly in two, seemingly remote, fields: (1) control devices as an alternative of electronics and (2) "power fluidic" for control of very hot aggressive and dangerous fluids. Nowadays the importance of fluidics seems to escalate in the both fields: an application of the fluidics in MEMS—microfluidic valves [18], and a gas turbine exhaust nozzle of high performance fighter/attack aircrafts [19]. An idea of oscillating jet, which is flipping by a control feedback loop as a fluidic oscillator, was suggested by Viets [20], Raman et al. [21], and recently in a different configuration without feedback loop by Mi and Nathan [22]. A two-dimensional oscillating impinging jet was designed on a fluidic principle by Herr and Camci [23], their main motivation was to improve a cooling of gas turbine blades.

An annular bistable nozzle with a fluidic control was designed recently by Peszyński [24]. The nozzle design was based primarily on an experience and intuition, a refinement of a geometry has been supported by an experimental as well as numerical investigations in follow-up variations [25,26]. Performance analysis of previous nozzle geometry has shown that more systematic approach based on collaborative experimental and numerical approaches can be very effective for the nozzle development. Moreover, an evident need of heat/mass transfer experiment has appeared. A combination of impinging jets with fluidics seems to be very promising for heat transfer enhancement. These were main motivations for the present experimental and numerical investigation of flow field, and for naphthalene mass transfer experiment.

## 2. Experimental facilities and techniques

Fig. 1 shows a schematic view of the present nozzle. The entire nozzle is situated horizontally and supplied by two independent airflow sources: the main flow is supplied by the centrifugal blower (2 kW) and controlled by a frequency regulator, control flow is supplied by the building compressor and controlled by a pressure regulator. Upstream of the nozzle, the main airflow passes through a horizontal tube, which has inner diameter and length 46 mm and 0.8 m, respectively. The control flow passes through a central tube, its outer diameter is 7.5 mm. The main nozzle is annular, its outside and inside exit diameters are $D = 84.0$ mm and $d = 74.0$ mm, respectively. The main nozzle contraction is 1.30 against the supply. The control nozzle is a radial slot of a width $\Delta_c = 0.5$ mm, its location is defined by a distance from the main nozzle exit, $x_c$ (see Fig. 1); three variants were studied with the $x_c$ of 0.0, 10.0, and 15.0 mm.

The nozzle is equipped with the spoiler (flow divider) and a ventilation slot (see Fig. 1), the geometry of both was designed during previous investigation. The spoiler is approximately parallel with the inner cone surface, its chord length and thickness are 5.0 and 0.35 mm, respectively. The spoiler is fixed by means of eight metal brackets (they are not plotted in Fig. 1), a location of the spoiler is defined by a distance from the main nozzle exit, $x_s$ (see Fig. 1). Three variants are presented here, the $x_s$ was 15.3, 20.0, or 25.0 mm. The ventilation is made by means of a slot of 1.5 mm wide, which is connected through 8 holes (diameter of each is 5 mm) with surroundings. The ventilation is optional, the

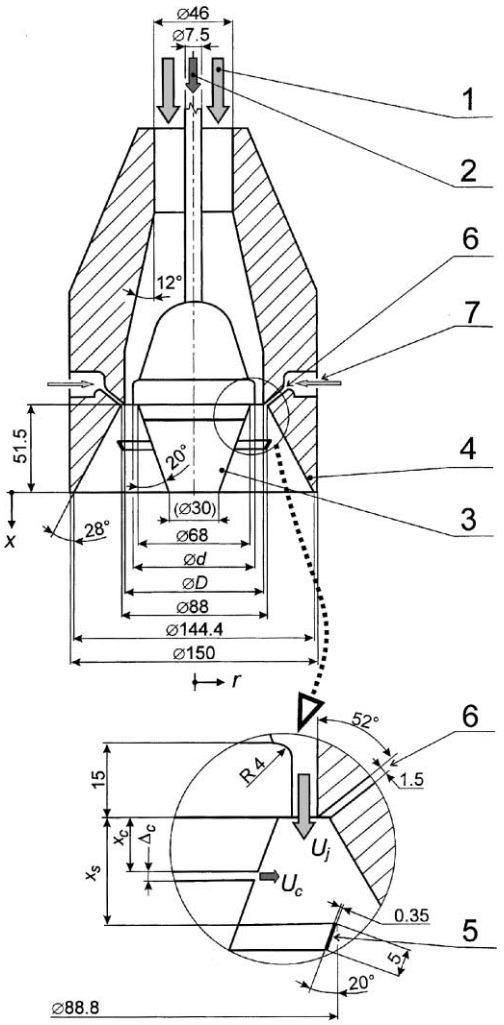


Fig. 1. Annular nozzle with a fluidic control, 1: main flow supply, 2: control flow supply, 3: inner nozzle cone, 4: outer nozzle cone, 5: spoiler, 6: ventilation slot, 7: optional ventilation (8 holes drilled equidistantly around the circumference, which connect the ventilation slot with surroundings; sometimes closed by Scotch tape). Dimensions: $D = 84$ mm, $d = 74$ mm, $\Delta_c = 0.5$ mm, $x_c = 0.0$, or 10.0, or 15.0 mm, $x_s = 15.3$, or 20.0, or 25.0 mm.

ventilation holes can be closed by the Scotch tape (it is stated in the text). A function of the spoiler and a ventilation slot is to suppress an undesirable hysteresis effect, which can occur during a jet switching; it will be discussed later.

The jet impingement is formed by a wall insertion across the jet axis. The wall for visualization and hot-wire experiment is made out of plywood, and it is covered with a plastic black foil. The wall for mass transfer experiments is a naphthalene plate as described below.

A smoke-wire technique similar to that of, e.g., Corke et al. [27], Fleisher et al. [9], was used for the visualization of air jet downstream the nozzle. Smoke-wire was made from three resistance wires with 0.1 mm in diameter, which were uniformly twisted together (it increases its surface and prolong the observation time, on the other hand a disruption of the flow increases a little bit only, 20% in hydraulic diameter). The smoke-wire was located horizontally across investigated jet axis. It was coated by paraffin oil before each test, and heated by Joule effect of direct current. The oil is evaporated from heated wire, and condensed by air stream rapidly. White filaments, which trace the airflow, are traditionally called a "smoke" (in fact, filaments consist of oil aerosol, i.e. of tiny droplets of oil with a typical diameter about 1 μm). Contrast white streaklines on black background was observed and photographed. Digital camera Olympus C-2500L Camedia was fixed 0.3–0.4 m above the nozzle, and oriented downwards. This configuration partly eliminates some buoyancy effect introduced into flow field visualization by the smoke-wire heating. Pictures were taken with a flashlight. A photoflash was located beside the nozzle, approximately in the smoke wire extension. It was equipped with a homemade optic system converging the light in the test section. The camera shutter release drove the flashlight, while the power supply to the wire was synchronized manually.

Both the main and control airflow rates are measured upstream the nozzle by a plate orifice and a rotameter, respectively. Both the main and control mean jet exit velocities ($U_j$ and $U_c$, respectively—see Fig. 1) were calculated from the airflow rates. A flow field measurement as well as computation were performed at the velocity range, $U_j = 8$–10 m/s; Reynolds numbers based on the annular nozzle outer diameter, and on its slot width, $Re_D$ and $Re_W$ were 42 000–53 000 and 2500–3100, respectively. On the other hand, the velocity was typically halved during the visualization, because of a limitation of the present smoke-wire technique.

Local velocity distribution of the jet was measured by a hot-wire anemometer (DANTEC, StreamLine System CTA90), which was operated in the constant temperature mode with the overheat ratio 1.15. The probe was a single sensor wire (DANTEC, model 55P16). One-axis traverse controlled by the PC was used to move the hot-wire probe in radial direction, an axial adjustment was made by a manual move of the traverse. The number of sampled data was 4096 points in each position. The sampling frequency was 1 kHz. The measured data were stored in the PC through NATIONAL INSTRUMENTS I/O board (AT-MIO-16E-10).

Two thermocouples of type K measure air temperature, they are located in the main supply tubing and in ambient. The other thermocouple was inserted in the nozzle exit before each test run, to be sure that experiments are made after equalization of temperature.

Local mass transfer was measured due to naphthalene sublimation from an exposed wall. The method was

described exhaustively by Goldstein and Cho [28], and authors' present variant has originated by Korger and Křížek [29]. Mass transfer experiment consists of three main steps: test specimens preparation, measurement, and data processing. Naphthalene test specimen is produced by a casting into a robust steel mold, an active surface is well polished and chromium-plated. Resultant naphthalene specimen has 130 mm × 450 mm active region, and 5.5 mm thickness.

Measurement of sublimate depth is performed in three steps, i.e., "before run" surface measurement, experiment run (test section is ventilated out of a laboratory), and "after run" surface measurement. The difference between the two sets of surface elevation is a resultant sublimation depth. The sublimation depth measurement system consist of XY table, eight depth gages (linear variation differential transformers) connected to signal conditioners (TOMES Krupka, Czech Republic), steppen-motor driven positioner, a hardware unit for motor control, and PC computer equipped with I/O board (NATIONAL INSTRUMENTS, AT–MIO–16E–10). Eight depth gages are traversed along the naphthalene specimen with an equidistant spacing 10 mm. Typical total number of data points are 2400, each of these points comprises an average of 10 partial sampling.

The local mass transfer coefficient is calculated from the sublimation depth [28] as

$$h_m = \frac{\rho_n R_n T_w \Delta x}{p_{sat} \Delta \tau}, \tag{1}$$

where $\rho_n$ is the density of solid naphthalene ($\rho_n = 1175$ kg/m$^3$ at 20 °C), $R_n$ is the gas constant for naphthalene ($R_n = 64.87$ J/(kg K)), $T_w$ is the exposed surface temperature in Kelvin, $\Delta x$ is net local sublimation depth, $p_{sat}$ is the saturated vapor pressure of naphthalene at the surface temperature [28], and $\Delta\tau$ is the duration run time. The extraneous sublimation due to natural convection (during the specimen manipulation and its surface measurement) has been evaluated by an auxiliary experiment, and is subtracted from the total sublimation depth; the resultant correction of the $h_m$-value was typically 0.0023 m/s. The maximum sublimation depth was 0.1 mm, a duration of the run time was 60–100 min. The saturated vapor pressure of naphthalene, $p_{sat}$, is calculated from Ambrose et al.'s empirical equation according to a recommendation [28]. The exposed surface temperature was evaluated from the temperature of air measured nozzle upstream, taking into account aerodynamic heating (recovery effect), and sublimation of the wall; the adiabatic naphthalene wall is assumed, i.e., the latent heat of sublimation comes from air. Wall temperature depression was typically 0.1–0.25 K against measured air temperature (it is not negligible value because of very high sensitivity of saturated vapor pressure to temperature).

Non-dimensional expression of mass transfer coefficient is the Sherwood number, $Sh_D = h_m D/D_n$, where $D$ is the characteristic length scale (outside diameter of annular nozzle exit), and $D_n$ is the mass diffusion coefficient of naphthalene vapor in air. The $D_n$ is calculated for measured temperature and pressure according to empirical equation suggested by Goldstein and Cho [28]. Based on the heat/mass transfer analogy [28], the mass transfer data can be converted to the corresponding heat transfer data by the following relation:

$$\frac{Sh_D}{Sc^n} = \frac{Nu_D}{Pr^n}, \tag{2}$$

where $Nu_D$, $Sc$, and $Pr$ are Nusselt, Schmidt, and Prandtl numbers. The exponent $n$ ranges 0.33–0.42, it can be determined from empirical results [1,2,28]. The $Sc$ is calculated for measured temperature according to empirical equation [28]; the typical value is 2.28 at 25 °C.

Uncertainty analysis was performed according to Kline and McClintock's method for single sample experiment [30]. The uncertainty of the solid naphthalene density $\rho_n$, temperature $T_w$, sublimation depth $\Delta z$, duration of test run $\Delta\tau$, nozzle diameter $D$, saturated vapor pressure $p_{sat}$, and mass diffusion coefficient $D_n$ were estimated 1.1%, 0.06%, 4.3%, 0.5%, 0.1%, 3.77%, and 5.1%, respectively. The uncertainty of the mass transfer coefficient and the Sherwood number is within 6% and 9% in the entire range of present measurements based on a 95% confidence level (±2 standard deviation).

## 3. Numerical modeling

### 3.1. Governing equations, CFD code and computing

The fluid flow is assumed to be axisymmetric, incompressible, isothermal, turbulent, and statistically stationary. The fluid properties (density and viscosity) are assumed to be constant. With these simplifications, the following set of equations govern the mean velocity flow field: continuity equation, time-averaged momentum (Navier–Stokes) equations, turbulent kinetic energy equation, and turbulent energy dissipation equation.

The flow fields is computed with the commercial finite-volume code FLUENT [31], in implicit formulation, in absolute velocities (computing of impinging jets by means of the same solver has been discussed recently by Garimella [8]). Continuity and momentum equation are coupled by the SIMPLE algorithm, which works in predictor–corrector steps, [32]. A standard scheme is used for the pressure discretization, and first order upwind is used in the momentum, turbulent kinetic energy, and turbulent energy dissipation equations. The multigrid method to accelerate the convergence, and iterative technique with under-relax predictions of the velocity and pressure are used. Default under-relaxation factors

of the solver were used, which are 0.3, 0.7, 0.8, and 0.8 for the pressure, momentum, turbulent kinetic energy, and turbulent energy dissipation, respectively. The results of iterations are evaluated by means of convergence criteria based on residual evolutions. The solution was considered to be converged when the sum of normalized residuals was less then $1 \times 10^{-3}$. The present computations were performed using multiprocessor Silicon Graphic computer, and usually took less then a half an hour for a task.

*Turbulence model, and the present near-wall modeling*. The Boussinesq turbulent–viscosity concept is incorporated with the renormalization group (RNG) $k$–$\varepsilon$ turbulence model—[31]. It has been chosen as sufficient for the present computation purposes, i.e. for a comparison of several variants, which are different in geometry or in control flow rates. The RNG $k$–$\varepsilon$ model is recommended for a stagnation flow computation—[31]. In comparison with more sophisticated models (Reynolds Stress Model and Large–Eddy Simulation model are available in FLUENT), the RNG $k$–$\varepsilon$ model requires relatively shorter computing time.

Near wall modeling is based on the standard wall function. It is assumed that two distinct fluid layers exist in the near-wall regions very close to the wall, namely a viscous sublayer up to $y^+ \sim 11.225$, and a fully turbulent logarithmic region above it—[31]. The former exhibits dominant molecular viscosity, latter dominant eddy viscosity, respectively. The default set of empirical constants was taken from [31]:

- $C_\mu = 0.0845$ (the eddy viscosity is calculated as $\mu_T = C_\mu \rho k^2/\varepsilon$),
- $C_{1\varepsilon} = 1.42$, $C_{2\varepsilon} = 1.68$ (the constants in the turbulent energy dissipation equation),
- $\beta = 0.012$, $\eta_0 = 4.38$ (the constants of the strain-dependent turbulent production in the turbulent energy dissipation equation).

### 3.2. The domain, grid, boundary conditions, and input data

Fig. 2 shows the computational domain and grid. Nozzle geometry was used basically the same as at experiments (see Fig. 1). The unstructured grid of triangles is being given with the use of symmetry in relation to the jet axis, the grid is generated by GAMBIT 1.3.0-generator associated with the solver. Numbers of volumes (2D axisymmetric zones) and nodes were 19 886 and 8208, respectively. A refined grid at the both main and control nozzles enables to capture a strong velocity gradient of the jet shear layers.

Grid independence was tested using the grid adaptation procedure of the FLUENT code. The grid was refined according to velocity gradients, and numbers of cells and nodes were increased 3.6–4.0 times. However,

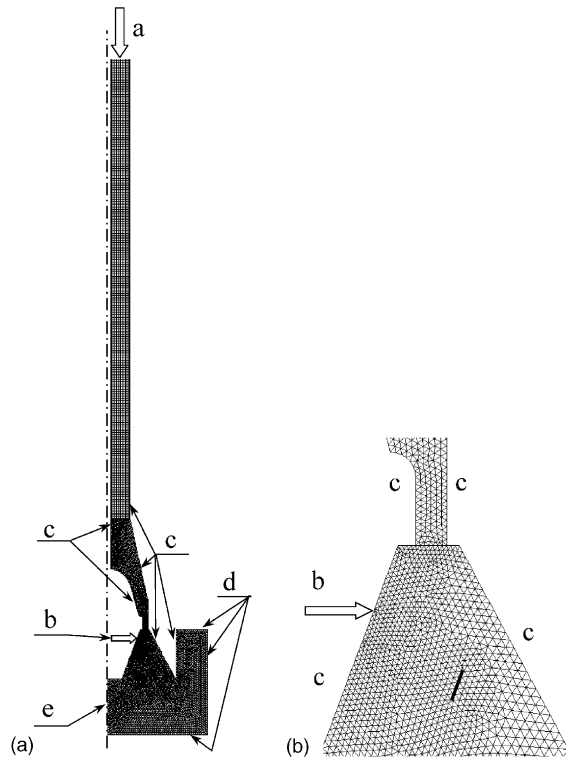


Fig. 2. Computational domain, grid, and boundary conditions: (a) entire domain, (b) detail of the grid near the nozzles and spoiler.

the problems with a convergence required to decrease all under-relaxation factors approximately into half-values. Thereafter a negligible effect on the computed flow field has been found—see Fig. 6(c) and (d), and a short comment at the end of paragraph 4.3.

The prescribed boundary conditions (a),(b),(c),(d),(e) are plotted in Fig. 2, and are as follows:

(a) Inlet of the main flow: since the tube length was set to be long enough (500 mm), the velocity profile at the inlet was set as uniform, $U_{\text{in}} = 6.52$ m/s (i.e., $U_{\text{j}} = 8.50$ m/s, $Re_D = 49\,400$, $Re_W = 2900$). The hydraulic diameter and turbulence intensity were chosen 40.8 mm and $k = 3\%$, respectively.
(b) Inlet of the control flow: the velocity profile at the control flow inlet was set as uniform, the velocity magnitude, $U_{\text{c}}$, were varied from 0 to 30 m/s. The turbulence intensity was chosen as $k = 3\%$.
(c) Walls, including the spoiler surface: a no-slip boundary condition was employed on the walls (all velocity components are zero).
(d) Outlet: a static pressure was prescribed as reference value, 98 000 Pa. It allows a recirculation flow (fluid enter of exit) at the outlet. The hydraulic diameter, and turbulence intensity (for fluid enter), were chosen 200 mm and 10%, respectively.

(e) Nozzle axis: standard symmetry conditions were employed.

Fluid properties of working fluid (air) were prescribed as follows: Fluid density, $\rho = 1.225$ kg/m$^3$; dynamic viscosity, $\mu = 1.7894 \times 10^{-5}$ kg/(m s).

### 3.3. The aim of the present numerical modeling

There are at least two essential advantages of numerical simulation of a jet impingement configuration, which have motivated the present approach. Firstly, a great number of parameters affect the complex flow field and the resulting heat/mass transfer. Better understanding of the flow field and heat/mass transfer processes requires to distinguish all of these effects. Apparently, to examine the effects separately by means of experiments is extraordinary difficult because of the task complexity. Moreover a comparison of experiments performed by different authors is often problematic, because of different experimental conditions (different facilities, laboratories, methods, etc.). On the contrary, a numerical approach to the complex problem can identify and quantify particular influences more easily.

Secondly, an experimental investigation focused on a jet impingement system needs typically a great number of experiments. The design of many geometry variants, their manufacturing and experimentation need some time as well as expenses. Obviously, numerical simulations can radically reduce the number of experimentally investigated variants.

The aim of the present numerical modeling is to evaluate the flow field sensitivity to the control jet, particularly to the control nozzle location, and to the control flow rate. The numerical modeling is considered as a basis for a design and manufacturing of a new geometry variants. The numerical solution can depend on methods and turbulence models, therefore it is meaningful to use it for relative comparisons (and with a careful interpretation). Results can be considered as reliable only if a proper experimental validation is carried out in a subsequent step.

## 4. Results and discussions

### 4.1. Fluidic control of the annular jet—two flow field states

Present annular jet is characterized by two flow field states—see Fig. 3:

- State 1, control jet is off. Air issuing from the main annular nozzle is inclined by means of Coanda Effect towards inner nozzle cone, reattaches some area of the cone surface, and continues along it. The resulting jet is focused along the nozzle axis.

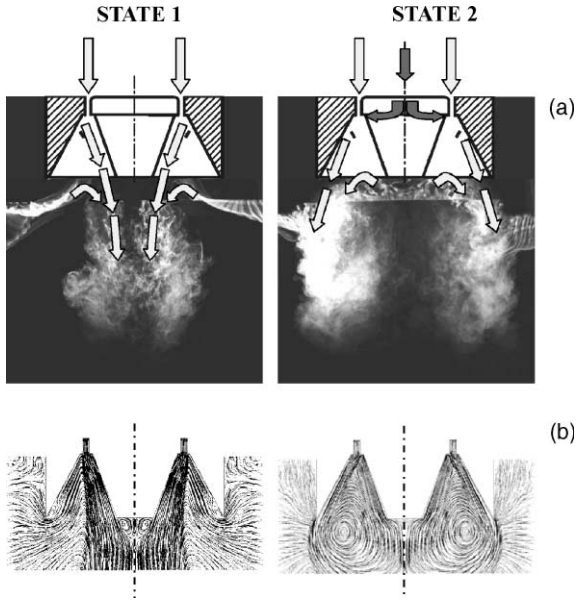


Fig. 3. Two states of the present annular jet, $x_c = 0$, without ventilation. (a) Smoke visualization at the $Re_D = 23000$, ($Re_W = 1400$, $U_j = 4.4$ m/s), $x_s = 15.3$ mm; $r_c = 0$ and 9.7% in states 1 and 2, respectively. (b) Computed pathlines at the $Re_D = 49400$ ($Re_W = 2900$, $U_j = 8.5$ m/s) without spoiler, $r_c = 0\%$ and 21.1% in states 1 and 2, respectively.

- State 2, control jet is on. Air issuing from the main annular nozzle is immediately forced by control jet toward outer nozzle cone, reattaches a surface of outer cone, and flows along it. The resulting jet is spread in diagonal direction out of outer cone edge. A cross section area of the jet is larger and velocity lower, as compared with state 1.

Fig. 3(a) shows flow visualization in the both states 1 and 2. Mean velocity in the nozzle exit was $U_j = 4.4$ m/s ($Re_D = 23000$), locations of the control nozzle and spoiler were $x_c = 0$ and $x_s = 15.3$ mm, respectively. The ventilation slot was closed. Visualized flow is turbulent, laminar–turbulent transition occurs inside the nozzle (it was not tested). In state 1 (control jet is off), surrounding air is entrained into the nozzle and the resultant jet is formed by inner nozzle cone along the nozzle axis. In state 2, the control jet is on ($r_c = 9.7\%$). An annular jet is formed by outer nozzle cone, air from central part is entrained backward into the nozzle and mixed with the main jet. Resulting jet is annular, and is spread out of outer cone edge. When the control jet was turned off, flow regime was returned immediately from state 2 to 1—the visualization proves a successful suppression of the hysteresis effect by means of the present spoiler.

Fig. 3(b) shows a typical result of numeric simulation, namely the distribution of the time–mean pathlines

in the states 1 and 2, at $Re_D = 44\,300$, $x_c = 0$; neither spoiler nor ventilation were used. A reason for practically half-value $Re_D$ of visualizations in Fig. 3 consists in experimental limits with visualization at higher flow velocities. Regardless, a qualitative comparison of experiments and computed flow field patterns is quite satisfactory.

It is worthy to note here that the nozzle geometry (Fig. 3(b)) was simplified and a spoiler was omitted. Despite this simplification, the flow sensitivity on a control jet action, and the ability to switch the main flow from state 1 to 2 can be estimated rather well. The following paragraph focuses on an efficient location of the control nozzle, and it uses this simplified geometry successfully too. On the other hand, a good enough prediction of a hysteresis behavior (such as a back-switching from state 2 to 1 at the control jet stopping) can be simulated only if the spoiler is taken into account—see paragraph 4.3.

### 4.2. Jet sensitivity on the control nozzle location

The motivation of this step is a consequence of the following contrast: the control jet has to be sufficient for a reliable jet state switching, but the control flow rate should be as small as possible (a typical low-energy demand).

A control nozzle location has been designed with a support of computing results. The most sensitive region of the flow field towards intended control jet action has been estimated near the reattachment region (see, e.g, a dotted arrow on Fig. 6(a)). Numerical simulation of the control nozzle locations $x_c = 0$, 10 and 15 mm was performed. Neither a spoiler nor ventilation were used. The control flow rate magnitude ($U_c$) was varied from 5–15 m/s (dimensionless control flow rate $r_c$ was 5–21%).

Fig. 4 shows computed pathlines. At a small control jet velocity, the flow field remains in state 1—similarly as without any control. If the control action is strong enough, the main flow is switched into state 2. The dotted polyline represents a boundary between states 1 and 2, which occur on the left and right hand side from the polyline, respectively. Fig. 4(b) shows clearly the best control nozzle location, namely the $x_c = 10$ mm, because the switching is achieved at the minimum control jet velocity ($U_c = 7.5$ m/s, i.e., $r_c = 9.4\%$). This result proves a high sensitivity of the flow field towards a control jet action near the reattachment region. Experimental confirmation is shown in the following text.

### 4.3. Switching characteristics: "jet switching" versus hysteresis effects

The description of the two flow states presented above does not take into account a gradual influence of the control flow on the main flow. Fig. 4 suggests that a

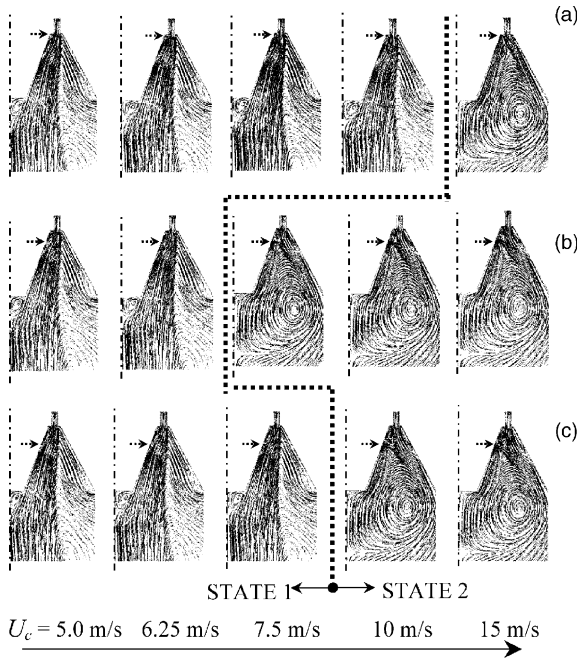


Fig. 4. Numerical simulation of a sensitivity of bistable flow field towards the control jet. The dotted polyline represents a boundary between states 1 and 2. Neither spoiler nor ventilation were used, $Re_D = 49\,400$. (a) $x_c = 0$, (b) $x_c = 15$ mm, and (c) $x_c = 20$ mm.

flow field is switched from state 1 in 2 at a certain jet control velocity. This concept of a jet switching is a simplification of a more complex real process, the switching between both states can be substantially complicated by means of hysteresis effects. In the following text is discussed, why rather complicated changes of the flow states can be considered as simply as jet switching, and which parameters are substantial for this consideration.

In fact, (A) a cycle of the jet switching from state 1 to 2 and back to 1 can be hysteretic in its character; (B) a moment of the jet switching is caused by the flow instability, thus the moment is preceded by a gradual forcing of the control jet and a gradual deflecting of the main jet.

Preliminary experiments were performed without any spoiler and ventilation, however, an undesirable hysteresis occurred. Although both flow field states 1 and 2 were stable, a deactivation of the control jet was not sufficient to switch state 2 into the state 1, and the jet remained (without spoiler and ventilation) in state 2 always, even without the flow control. To eliminate this unwanted hysteresis behavior, the nozzle was equipped with the spoiler. Moreover, a ventilation slot was tested.

(A) Fig. 5(a) shows the switching characteristics in the form of $U$–$r_c$ relationship. The velocity $U$ was measured approximately in a position of the jet in state

1; the position was found by means of flow visualization typically as $x = 40$ mm, $r = 15$ mm (except Fig. 5(b)). The control flow rate $r_c$ was gradually increased in small steps, and the UP-curve of Fig. 5(a) shows that a change from the jet state 1 to 2 occurs at the $r_c = 9.2$–$9.5\%$. A return from state 2 to 1 occurs during a gradual decreasing of the $r_c$ at the $r_c = 8.4$–$9.0\%$ (DOWN-curve). An overlapping of both curves demonstrates illustratively a hysteresis effect. This effect is relatively small because of a proper spoiler function: if the jet is in state 2, the spoiler deflects permanently a small part of the jet centripetally, thus it counteracts the control flow effect. A detail of computed pathlines inside the nozzle will be discussed according to Fig. 6(b) below. On the other hand, the main air stream in state 1 passes the spoiler, thus an influence of the spoiler is very small in state 1.

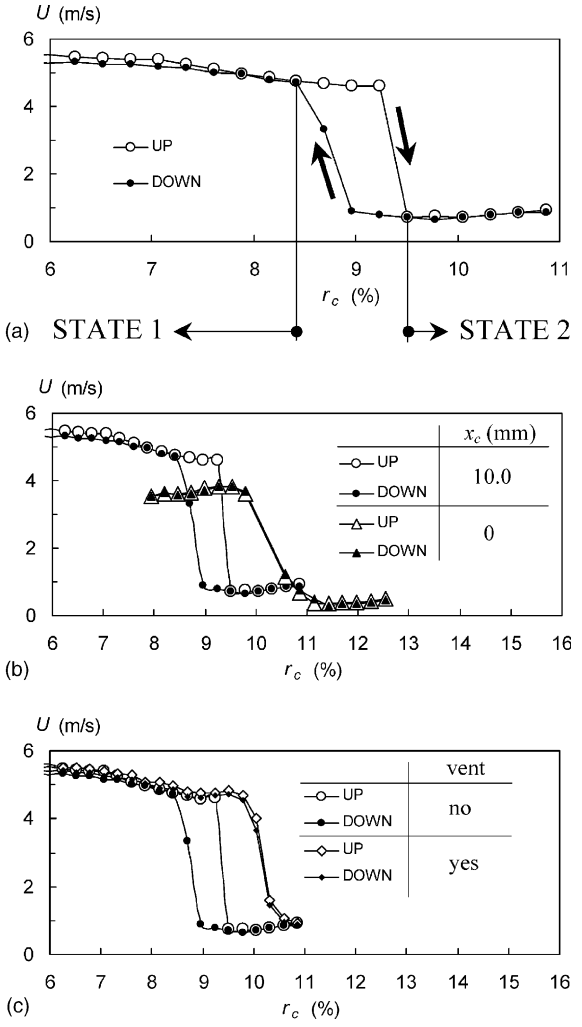


Fig. 5. Jet switching, experiments at $Re_D = 43\,000$ ($U_j = 8.2$ m/s); (a) $x_c = 10$ mm, $x_s = 20$ mm, without ventilation, (b) effect of a control nozzle location, and (c) ventilation effect.

(B) Further, Fig. 5(a) shows some gradual decrease of the measured velocity with the increasing control rate in the whole range of state 1. It is caused by a gradual deflecting of the main flow out of the inner cone, which is caused by the control jet forcing. On the contrary, a very small gradual increase of the $U$ occurs in state 2—the main reason can be a positive contribution of control flow rate to the mass balance of the resultant flow.

Both jet states 1 and 2 are denoted in Fig. 5(a), they occur at the control flow rate $r_c < 8.4\%$ and $r_c > 9.5\%$, respectively. An interjacent range $r_c = 8.4$–$9.5\%$ is linked with hysteresis effects and with a dynamic behavior of the unsteady flow near its instability.

Fig. 5(b) compares two variants of control jets location, $x_c = 0$ and 10 mm. The location $x_c = 0$ mm is evidently less effective because the jet switching occurs at a higher control flow rate (lower velocities for the $x_c = 0$ were measured by a different location of the CTA-probe, thus are not relevant to the present explanation of jet switching).

Fig. 5(c) shows the influence of the ventilation slot (see Fig. 1). Relatively small hysteresis range is fully eliminated by means of the ventilation. On the other hand, the control flow rate increases a bit because of the ventilation. In other words, the jet switching with the ventilation is more robust, because the hysteresis effects are completely eliminated. However, the jet switching is a bit more effective without the ventilation when the control flow rate is approximately 1% lower. The ventilation slot counteracts the control flow effect similarly as the spoiler. The reason is that a separation region (bubble) occurs in state 2 between the outer annular nozzle lip and outer cone (see Fig. 6(b) below). The pressure throughout this region is basically less than of the jet. This underpressure is caused by the jet itself, specifically by means of its entrainment from surroundings (Coanda Effect). The underpressure can cause a curvature of the jet into state 2 even without any active jet control. The ventilation slot allows air entrainment inward the separation bubble, thus a pressure is partially equalized there, which results in curvature weakening.

Fig. 6(a) and (b) show the controlled jet inside the nozzle in detail. Computed mean pathlines are plotted for states 1 and 2, respectively. The result shows the proper function of the spoiler:

- In state 1 (Fig. 6(a)), the main air stream passes the spoiler, thus its influence is relatively small.
- In state 2 (Fig. 6(b)), the spoiler deflects permanently a small part of the jet centripetally. The resultant complex flow field structure with many large vortices is not studied in detail for the time being, a sufficient result is that the spoiler in state 2 counteracts the centrifugal control flow effect effectively, as proved experimentally.

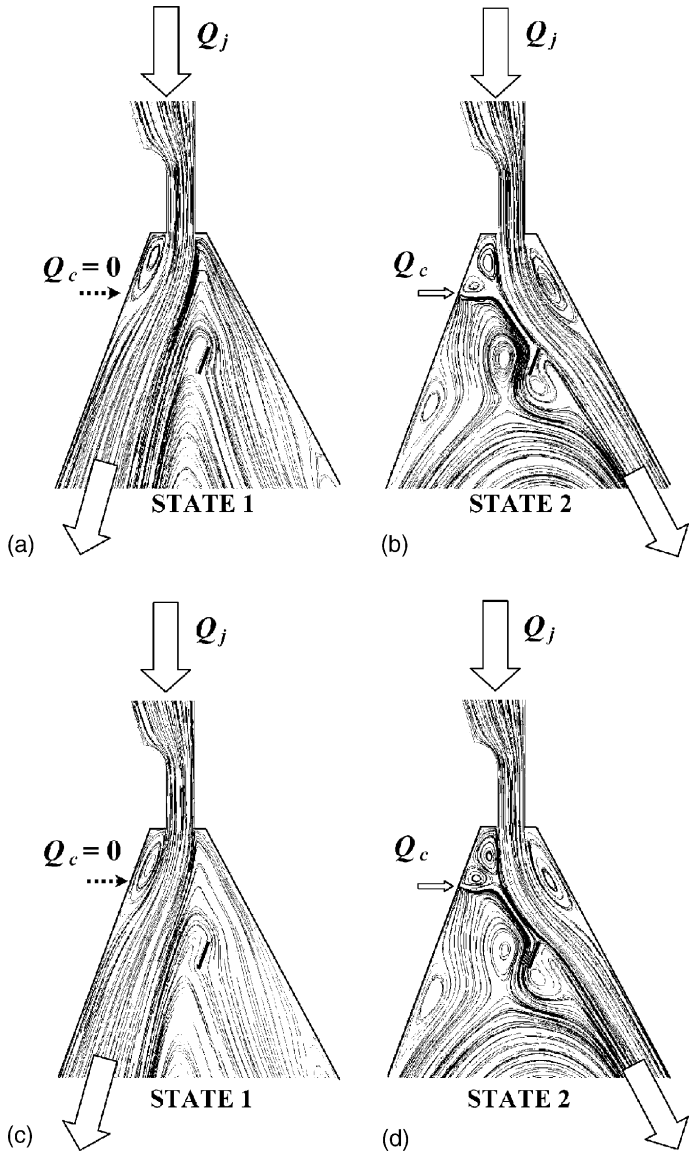


Fig. 6. Computed mean pathlines inside the nozzle in detail, $Re_D = 49\,400$, $x_c = 10$ mm, $x_s = 20$ mm, without ventilation. (a) State 1, control is off, $r_c = 0$; (b) state 2, control is on, $r_c = 10.9\%$; (c) repeated computation of state 1 using a refined grid; (d) repeated computation of state 2 using a refined grid.

Fig. 6(c) and (d) show results of computation performed using a refined grid, when numbers of cells and nodes have been increased 3.6–4.0 times. A comparison with Fig. 6(a) and (b) demonstrates that an effect of the grid on computed flow fields can be neglected (differences in vortex structures lie outside a scope of this work).

The final variant of the present nozzle has been equipped with the spoiler and ventilation slot, see Fig. 1. The hysteresis effect has been suppressed. In other words, a switching from state 2 to 1 occurs immediately after a deactivation of the control jet, i.e. the spoiler and ventilation "spoil" together state 2.

### 4.4. Mean flow fields

Fig. 7(a) and (b) show computed and measured velocity magnitude profiles, respectively. Left column of figures shows state 1 (flow control off, $r_c = 0$), right column shows state 2 (flow control on, $r_c = 10.9\%$). The computation and experiments are in quite good qualitative agreement. The results correspond to the present

concept of fluidic control—the jet is focused along the nozzle axis in state 1, or it is spread out in state 2. It is worth underlining here that this good agreement between the computed and measured results of fluidic control is an essential point for the present work.

Fig. 7 shows that a quantitative agreement is satisfactory in state 1. On the other hand, differences between computation and experiment are much bigger in state 2—a computed span of the velocity maxima is smaller than a measured one, thus the computed separation bubble is smaller. A reason can be that the present computation is focused on the jet switching, and the present domain follows this aim. However, the present domain is too small for a correct computation of an annular jet development. Therefore an outlet of the domain is under a very strong influence of a large recirculation flow, and the computation near the outlet does not agree with measurement.

### 4.5. Annular impinging jet—mass transfer experiments

Fig. 8(a)–(c) show the results of the experiments with impinging annular jets, namely flow field scheme, smoke visualization, and a mass transfer distribution, respectively. Nozzle-to-wall spacing, $H$, was 80 mm. Mass transfer coefficient has been transformed into dimensionless form ($Sh$), and recalculated into the common ratio of $Sh_D/(Re^m Sc^n)$. Exponents were chosen $m = 0.7$, $n = 0.4$. The former exponent reasonably complies with the impinging jet behavior [1,2] (however, present work does not study an influence of the Reynolds number in detail). The latter exponent typically ranges 0.33–0.42 (e.g. the $n = 1/3$ on a flat plate in laminar flow), and is commonly accepted in heat/mass transfer analogy [1,28]. Therefore, the present mass transfer data from Fig. 8(c) are applicable for heat transfer prediction through the analogy (2) as

$$\frac{Sh_D}{Re_D^{0.7} Sc^{0.4}} = \frac{Nu_D}{Re_D^{0.7} Pr^{0.4}}. \tag{3}$$

The reason for using approximately half of $Re_D$ in visualization experiments is that there are experimental difficulties at higher flow velocities (otherwise, the naphthalene sublimation is problematic at small velocities). Preliminary visualization experiments show that a qualitative behavior of flow fields (jet switching) is independent on the Reynolds number in the present $Re_D$ range. Left column of Fig. 8 shows state 1 (flow control off), right column shows state 2 (flow control on):

Annular impinging jet in state 1—flow control off. A recirculation region behind inner cone does not bridge the whole nozzle-to-wall space completely, flow field near the central stagnation point qualitatively resembles a basic case of a round impinging jet. Stagnation point on the wall is located in the point of intersection of the nozzle axis with a wall, no other stagnation point is on the wall. On the other hand, jet impinging onto the wall is basically undeveloped because of relatively short nozzle-to-wall spacing. Velocity profiles are apparently saddle formed with a minimum on the axis, therefore the mass transfer profile is saddle formed too. This annular impinging jet is usually referred to as the "closed type pattern" in [13], or the "centrifugal case" in the recent paper [17]. The latter name seems to be more

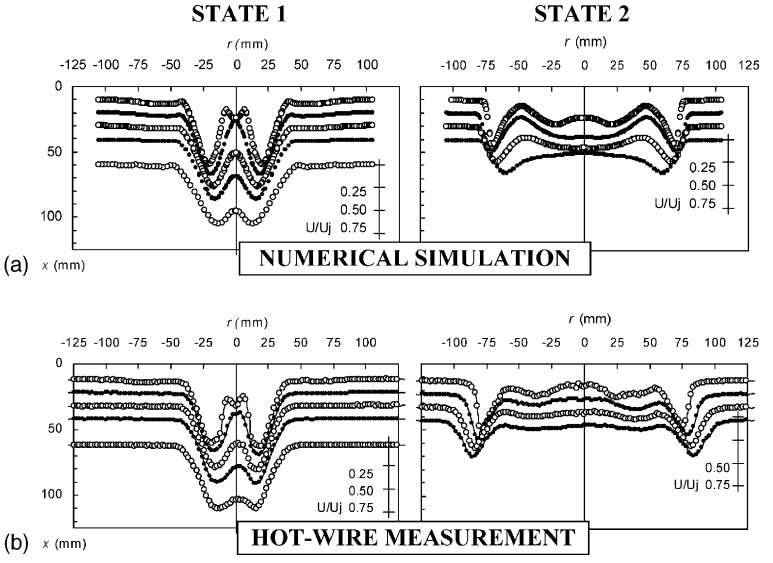


Fig. 7. Velocity magnitude profiles. Left column of figures shows the state 1 (flow control off, $r_c = 0$; $x = 10$, 20, 30, 40, 60 mm), right column shows the state 2 (flow control on, $r_c = 10.9\%$; $x = 10$, 20, 30, 40 mm); $x_c = 10$ mm, $x_s = 20$ mm, without ventilation; (a) computation at $Re_D = 49\,400$ and (b) measurement at $Re_D = 42\,000$.

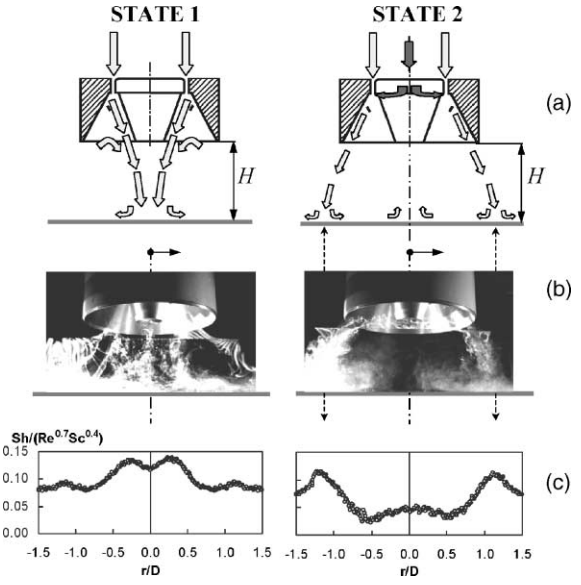


Fig. 8. Annular impinging jet. Left column of figures shows the state 1 (flow control off, $r_c = 0$), right column shows the state 2 (flow control on, $r_c = 9.7\%$ and 6.5% for visualization and mass transfer experiments, respectively); $H = 80$ mm, $x_c = 0$, $x_s = 15.3$ mm, without ventilation. (a) Flow field scheme, (b) smoke visualization at the $Re_D = 23\,000$, and (c) mass transfer on an exposed wall at the $Re_D = 52\,800$ and 49 600 ($U_j = 10.1$ and 9.5 m/s) in the states 1 and 2, respectively.

apt—streamlines on the exposed wall run away from the central stagnation point.

Annular impinging jet in state 2—flow control on. Nozzle-to-wall space is filled up with a separation bubble flow, all recirculation region is bordered by annular jet issuing from nozzle. This annular impinging jet is referred to as the "open type pattern" in [13], or the "reverse stagnation point" in [14]. Recently, this flow pattern has been called more aptly as the "centripetal case" in [17]—wall streamlines run from an outer stagnation circle towards the central (reverse) stagnation point.

Similarly with a non-impinging jet case, hysteresis effects can be neglected in the impinging jet case because of a proper function of the present spoiler.

*Remark:* The present nozzle (Fig. 1) could be used with a periodic forcing to create oscillating (impinging) jets. This possibility is one of the reasons for a present effort to eliminate hysteresis effects. It is a generally accepted fact that periodic oscillations can potentially lead to a heat transfer enhancement. However, the oscillations do not imply this effect (for the impinging jets) automatically, heat transfer can sometimes increase, sometimes decrease (or the effect is little)—see [11]. A natural unsteady behavior of stagnation points is well known, large-scale fluctuations were studied even at annular impinging jets [14]. It should be helpful to correlate these natural fluctuations with a periodic external forcing. However, the present investigation deals with steady flow solely, a periodic forcing lies outside the scope of this work. In any case, heat transfer enhancement by means of the present nozzle with a periodic forcing seems to be a promising task for the future.

## 5. Conclusions

Numerical and experimental investigation of an annular actively controlled jet have been performed in several subsequent steps. A design fundamental has been already known from the previous experimental study. Sequentially, a numerical simulation (using a commercial CFD code FLUENT 5.5.14) has given a basis for a geometry adaptation, and for new model design and manufacturing. Flow visualization has allowed an adjustment of a desirable flow field patterns, and it has proved a proper switching of flow field states. Further, hot-wire measurement has confirmed and refined an estimation of flow field states, and it has produced data for a quantitative analysis. Finally, naphthalene sublimation experiment has rendered data (local mass transfer coefficient) for an evaluation of heat/mass transfer onto exposed walls.

Better locations of a control jet and a spoiler have been designed. The former decreases a control flow rate, the latter suppresses a hysteresis effect. A function of a ventilation slot has been tested. The jet switching with the ventilation is more robust and a hysteresis can be completely eliminated. However, jet switching is evidently more effective without any ventilation when a control flow rate is approximately 1% lower.

The present work proves that even a standard commercial CFD solver can be used for simulation of the both states of bistable impinging jet. However, an interpretation of the numerical results is not self-explanatory, typically under a hysteresis influence. The present work demonstrates that numerical solution is very useful and attractive for a design optimization, however, results are necessary to be interpreted with a particular caution. Specifically, an occurrence or suppression of hysteresis effects has been proved unambiguously by experiments in this work.

The results proved bistable behavior of the (non-impinging as well as impinging) jets, and a proper function of the fluidic control including a suppression of an unwanted hysteresis at a jet state switching. A yield of collaborative numerical and experimental investigations lies in a better understanding of mechanisms involved in controlled impinging jets, as well as in a beneficial improvement of the particular nozzle geometry. The results are considered to be significant for a heat/mass transfer augmentation of impinging jets in the near future. Moreover, a generation of oscillating impinging jets is

consistent with the present fluidic control including the proposed treatment of hysteresis effects. It has been suggested that the periodic forcing can potentially lead to a desirable enhancement of impinging jets.

## Acknowledgements

We gratefully acknowledge the support by the Grant Agency of the Academy of Sciences of the Czech Republic (project no. A2076301) and by the State Committee for Scientific Research, Poland (project no. Z/19/3/98, ATR BW-8/98).

## References

[1] E.P. Dyban, A.I. Mazur, Convection Heat Transfer in Impinging Jets (Konvektivnyj teploobmen pri strujnom obtekanii tel), first ed., Naukova dumka, Kiev, 1982 (in Russian).
[2] H. Martin, Heat and mass transfer between impinging gas jets and solid surfaces, Adv. Heat Transfer 13 (1977) 1–60.
[3] S.J. Downs, E.H. James, Jet impingement heat transfer—a literature survey, in: Proceedings of the National Heat Transfer Conference, ASME, Pennsylvania, PA, 1987, 87-HT-35.
[4] K. Jambunathan, E. Lai, M.A. Moss, B.L. Button, A review of heat transfer data for single circular jet impingement, Int. J. Heat Fluid Flow 13 (2) (1992) 106–115.
[5] R. Viskanta, Heat transfer to impinging isothermal gas and flame jets, Exp. Thermal Fluid Sci. 6 (1993) 111–134.
[6] S. Polat, Heat and mass transfer in impinging drying, Drying Technol. 11 (6) (1993) 1147–1176.
[7] B.W. Webb, C.-F. Ma, Single-phase liquid jet impingement heat transfer, Adv. Heat Transfer 26 (1995) 105–107.
[8] S.V. Garimella, Heat transfer and flow fields in confined jet impingement, Ann. Rev. Heat Transfer XI (2000) 413–494.
[9] A.S. Fleischer, K. Kramer, R.J. Goldstein, Dynamics of the vortex structure of a jet impinging on a convex surface, Exp. Thermal Fluid Sci. 24 (2001) 169–175.
[10] R.J. Goldstein, E.R.G. Eckert, W.E. Ibele, S.V. Patankar, T.W. Simon, T.H. Kuehn, P.J. Strykowski, K.K. Tamma, A. Bar-Cohen, J.V.R Heberlein, J.H. Davidson, J. Bischof, F.A. Kulacki, U. Kortshagen, S. Garrick, Heat transfer—a review of literature, Int. J. Heat Mass Transfer 45 (14) (2002) 2853–2957.
[11] C. Herman, The impact of flow oscillations on convective heat transfer, Ann. Rev. Heat Transfer XI (2000) 495–562.
[12] V. Narayanan, J.S. Yagoobi, R.H. Page, Heat transfer characteristic of a slot jet reattachment nozzle, Trans. ASME J. Heat Transfer 120 (1998) 348–356.
[13] Y. Kokoshima, A. Shimizu, T. Murao, Numerical analysis of annular turbulent jet impinging on a flat plate, in: Proceedings of the 3rd Triennial International Symposium on Fluid Control, Measurement, and Visualization, FLUCOME '91, ASME, San Francisco, 1991, pp. 205–210.
[14] H. Maki, A. Yabe, Unsteady characteristics of the annular impinging jet flow field and reverse stagnation point heat transfer, in: Proceedings of the National Heat Transfer Conference Heat Transfer in Convective Flows, Philadelphia, PA, 1989, HTD-vol. 107, pp. 163–168.
[15] Z. Trávníček, F. Křížek, Impinging jet and combined slot nozzle (Impaktströmung und die Zusammengesetzte Schlitzdüse), Heat Mass Transfer 35 (5) (1999) 351–356 (in German).
[16] Z. Trávníček, F. Maršík, Flow visualization and mass transfer with a bistable two-slot impinging jet, in: Proceedings of the 10th International Symposium of the Flow Visualization (ISFV 10), Kyoto, 2002, Book of Abstracts p. 44; Full text CD-ROM, F0068.
[17] V. Tesař, M. Jílek, Z. Randa, Topology changes in an annular impinging jet flow, in: Proceedings of the Topical Problems in Fluid Mechanics 2001, Institute of Thermomechanics CAS, Prague, 2001, pp. 121–124.
[18] V. Tesař, Microfluidics for MEMS—microfluidic valve, in: F.B. Hsiao (Ed.), Proceedings of the 4th Pacific International Conference on Aerospace Science and Technology, Kaohsiung, Taiwan ROC, 2001, pp. 301–305.
[19] J.F. Federspiel, L.S. Bangert, D.J. Wing, T. Hawkes, Fluidic control of nozzle flow-some performance measurements, in: Proceedings of the 31st AIAA/ASME/SAE/ASEE Joint Propulsion Conference, San Diego, CA, 1995, AIAA Paper No. 95-2605.
[20] H. Viets, Flip–flop jet nozzle, AIAA J. 13 (10) (1975) 1375–1379.
[21] G. Raman, E.J. Rice, D.M. Cornelius, Evaluation of flip–flop jet nozzles for use as practical excitation devices, Trans. ASME, J. Fluids Eng. 116 (1994) 508–515.
[22] J. Mi, G.J. Nathan, New flip–flop jet nozzle without control port and feedback loop, in: E. Lindborg et al. (Eds.), Proceedings of the 2nd Int. Symposium Turbulence and Shear Flow Phenomena (TSFP-2), Stockholm, vol. II, 2001, pp. 253–257.
[23] F. Herr, C. Camci, Self-oscillating-impinging-jet as a gas turbine cooling enhancement system, in: Proceedings of the International Gas Turbine & Aeroengine Congress & Exposition, ASME, Orlando, FL, 1997.
[24] K. Peszyński, Flow control by axisymmetric fluidic device with radial switching, in: Proceedings of the Engineering Mechanics '98, Czech Academy of Sciences, Svratka, Czech Republic, 1998, pp. 583–588.
[25] K. Peszyński, J. Hošek, Z. Kuszyński, Z. Trávníček, S. Wawrzyniak, Active control of annular bistable jet, in: Proceedings of the Engineering Mechanics 2000, Czech Academy of Sciences, Svratka, Czech Republic, 2000, vol. IV, pp. 149–154.
[26] K. Peszyński, Z. Trávníček, Jet flow visualization for an axi-symmetric nozzle, in: J. Sempruch (Ed.), Development in Control and Machinery Design, Wydawnictwa Uczelniane Akademii Techniczno-Rolniczej, Bydgoszcz, 2002, pp. 55–64.
[27] T. Corke, D. Koga, R. Drubka, H. Nagib, A new technique for introducing controlled sheets of smoke streaklines in wind tunnels, in: Proceedings of the 7th International Congress on Instrumentation in Aerospace Simulation Facilities (ICIASF '77), IEEE Publication 77CH 1251-8 AES, Royal Military College of Science, Shrivenha, 1977, pp. 74–80.

[28] R.J. Goldstein, H.H. Cho, A review of mass transfer measurements using naphthalene sublimation, Exp. Thermal Fluid Sci. 10 (1995) 416–434.
[29] M. Korger, F. Křížek, Mass-transfer coefficient in impingement flow slotted nozzles, Int. J. Heat Mass Transfer 9 (5) (1966) 337–344.
[30] S.J Kline, F.A. McClintock, Describing uncertainties in single-sample experiments, Mech. Eng. 75 (1953) 3–8.
[31] FLUENT User's Guide, Release 5.5.14. FLUENT Inc., Lebanon, 1998.
[32] S.V. Patankar, Numerical Heat Transfer and Fluid Flow, Hemisphere, Washington, DC, 1980.